U.S. ARMY COMBAT CAPABILITIES DEVELOPMENT COMMAND
CHEMICAL BIOLOGICAL CENTER
ABERDEEN PROVING GROUND, MD 21010-5424

DEVCOM CBC-TR-1830

Nanofluids for Displacement of Entrained Contaminants from Restricted Geometries

Mark J. Varady
Brent A. Mantooth
Neil Hawbaker
RESEARCH AND OPERATIONS DIRECTORATE

Adam R. Hinkle
DCS CORPORATION
Belcamp, MD 21017-1561

Melissa S. Hulet
Jill Ruth
LEIDOS, INC.
Reston, VA 20190-5617

Melissa L. Sweat
DEFENSE THREAT REDUCTION AGENCY
Fort Belvoir, VA 22060-6201

April 2023

Disclaimer

The findings in this report are not to be construed as an official Department of the Army position unless so designated by other authorizing documents.

REPORT DOCUMENTATION PAGE

1. REPORT DATE	2. REPORT TYPE	3. DATES COVERED	
		START DATE	END DATE
XX-04-2023	Final	Oct 2021	Sep 2022

4. TITLE AND SUBTITLE
Nanofluids for Displacement of Entrained Contaminants from Restricted Geometries

5a. CONTRACT NUMBER	5b. GRANT NUMBER	5c. PROGRAM ELEMENT NUMBER
5d. PROJECT NUMBER	**5e. TASK NUMBER**	**5f. WORK UNIT NUMBER**
PE 0601102A project VR9		

6. AUTHOR(S)
Varady, Mark J.; Mantooth, Brent A.; Hawbaker, Neil* (DEVCOM CBC); Hinkle, Adam R. (DCS); Hulet, Melissa S.; Ruth, Jill (Leidos); and Sweat, Melissa L. (DTRA)

7. PERFORMING ORGANIZATION NAME(S) AND ADDRESS(ES)
Director, DEVCOM CBC, ATTN: FCDD-CBR-PD, APG, MD 21010-5424
Defense Threat Reduction Agency; 8725 John J. Kingman Road, MSC 6201, Fort Belvoir, VA 22060-6201
Leidos, Inc.; 1750 Presidents Street, Reston, VA 20190-5617
DCS Corporation; 4696 Millennium Drive, Suite 450, Belcamp MD 21017-1561

8. PERFORMING ORGANIZATION REPORT NUMBER
DEVCOM CBC-TR-1830

9. SPONSORING/MONITORING AGENCY NAME(S) AND ADDRESS(ES)	10. SPONSOR/MONITOR'S ACRONYM(S)	11. SPONSOR/MONITOR'S REPORT NUMBER(S)
U.S. Army Combat Capabilities Development Command Chemical Biological Center; 8198 Blackhawk Road; Aberdeen Proving Ground, MD 21010-5424	DEVCOM CBC	

12. DISTRIBUTION/AVAILABILITY STATEMENT
Distribution Statement A. Approved for public release: distribution unlimited.

13. SUPPLEMENTARY NOTES
*Neil Hawbaker is currently affiliated with Scale-Up Systems (Dublin, Ireland) and is no longer affiliated with DEVCOM CBC.

14. ABSTRACT (LESS THAN 200 WORDS)
Liquid-phase chemical warfare agent can become entrained in constrained geometries (capillary features) on military assets (e.g., screw threads or between mated surfaces). If the liquid contaminant wets the solid, capillary forces stabilize the contaminant, and conventional decontaminants are ineffective. This work seeks to leverage research in the field of enhanced oil recovery, in which nanofluids are used to displace oil trapped in underground rock formations. Two types of nanofluids are studied here: (1) a reactive, sodium-based nanofluid and (2) silica and polyethylene glycol (PEG)-based nanofluids that promote contaminant dewetting. It was found that the sodium nanofluid is effective at displacing contaminant by gas bubble formation and expansion, providing a force that pushes against the contaminant. The silica- and PEG-based nanofluids were effective at dewetting contaminant from capillary walls relative to aqueous surfactant-based controls but did not remove the contaminant from the capillary. It was found that the silica nanofluids form a pore network upon water evaporation, and contaminant trapped in an adjacent capillary can be passively pulled out of the capillary feature into this pore network. Further study of this mechanism and how it can be coupled with the dewetting capability of silica nanofluids is suggested.

15. SUBJECT TERMS
Decontamination; Chemical warfare agent (CWA); Capillary displacement; Nanofluids
Entrainment; Enhanced oil recovery (EOR); Complex features

16. SECURITY CLASSIFICATION OF:			17. LIMITATION OF ABSTRACT	18. NUMBER OF PAGES
a. REPORT	b. ABSTRACT	C. THIS PAGE		
U	U	U	UU	30

19a. NAME OF RESPONSIBLE PERSON	19b. PHONE NUMBER *(Include area code)*
Renu B. Rastogi	(410) 436-7545

Blank

PREFACE

The work described in this report was authorized by the Chemical Biological Advanced Materials and Manufacturing Science Program at the U.S. Army Chemical Combat Capabilities Development Command Chemical Biological Center (DEVCOM CBC) under project number PE 0601102A project VR9. The work was started in October 2021 and completed in September 2022.

The use of either trade or manufacturers' names in this report does not constitute an official endorsement of any commercial products. This report may not be cited for purposes of advertisement.

This report has been approved for public release.

Acknowledgments

The authors acknowledge the following individuals for their hard work and assistance with the execution of this technical program:

- DEVCOM CBC Decontamination Sciences Branch members for their efforts in performing this study; and
- Dr. Charles Bass and Dr. Bernadette Higgins of the Defense Threat Reduction Agency (Fort Belvoir, VA) for their interest and conversations related to this work.

Blank

CONTENTS

FIGURES

TABLES

NANOFLUIDS FOR DISPLACEMENT OF ENTRAINED CONTAMINANTS FROM RESTRICTED GEOMETRIES

1. INTRODUCTION

1.1 Motivation

Much of the research on decontamination of materials exposed to chemical warfare agents (CWAs) has focused on the ideal case of a flat, horizontally oriented material surface. However, real military assets have complex features with small gaps resulting from mated surfaces, discontinuities, and screw threads, for example, as shown in Figure 1. When liquid-phase CWA wets a material of interest, capillary forces can pull the CWA into these small gaps. Once the CWA is stabilized in such a capillary feature, it is difficult to remove; interaction with a decontaminant is limited by the exposed surface area, which can be extremely small. Figure 1 shows a schematic of liquid agent entrained in a simple capillary feature and illustrates how the capillary force and available interaction area scale with the capillary size. Both capillary and viscous forces become greater as the size of the capillary decreases and the liquid becomes more difficult to remove. Similarly, the available interaction area decreases, which diminishes the rates of agent evaporation, dissolution, and reaction taking place at the capillary entrance.

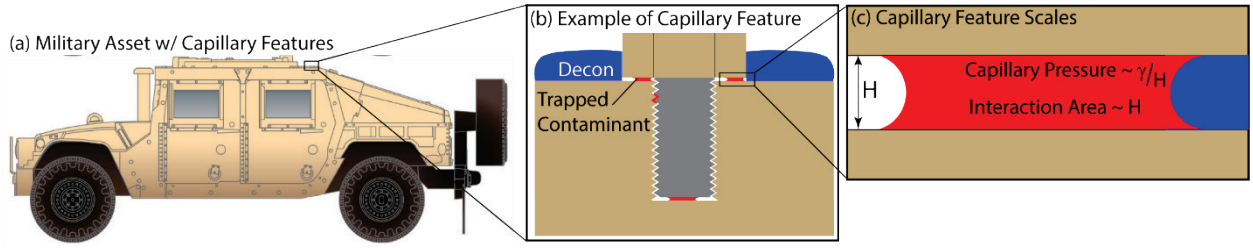

Figure 1. (a) Military asset with (b) magnified view of example capillary feature formed by mating of a screw with a surface and (c) depiction of how capillary pressure and interaction scales with capillary size. Red indicates contaminant; blue indicates decontaminant. *H*, height.

This transport limitation severely diminishes the effectiveness of typical decontamination treatments. In recent work, the vapor emissions of a CWA simulant from various sizes of capillary features were examined, with and without a standard rinse treatment.[1] It was found that the vapor emission from capillaries below a certain size threshold (~100 μm) was unaffected by the rinse process. Currently, work is ongoing to quantify the hazard from capillary-entrained agent relative to other sources on military assets (e.g., liquid on surface or absorbed in polymer-based paint coatings) and the effectiveness of different decontamination treatments (e.g., reactive slurry and hot air flow). Results indicate that capillary-entrained CWA can account for a significant fraction of total residual CWA after a decontamination treatment, and that various decontamination treatments are ineffective for smaller capillaries.

One strategy for overcoming the transport limitations imposed by the capillary-entrained agent is to remove the agent from the capillary so that the decontaminant can optimally contact the agent. Finding effective techniques for removing CWA from a capillary feature is potentially a difficult problem requiring a significant research investment. Fortunately, a significant body of research exists that can be leveraged in the field of enhanced oil recovery (EOR), where the goal is to displace and recover oil trapped in underground rock pores, where it is stabilized by strong capillary and viscous forces. The similarity in physics between capillary-entrained CWA and EOR motivates the application of techniques developed for EOR to CWA decontamination, which is the focus of this work.

1.2 Nanofluids for EOR

After the primary (drilling and pumping) and secondary (water flooding) oil recovery processes are complete, up to 50% of the original oil in place remains trapped in the underground rock formations and held by strong capillary and viscous forces.[2] Development of effective EOR methods to recover this elusive oil is an active area of research, and no method has clearly emerged as the best. The use of a high-temperature fluid such as steam to lower the oil viscosity and surface tension[3] or high-pressure gas injection to push the oil from the pores[4] represent energy-intensive processes that are impractical for CWA decontamination. Of interest for decontaminant development are the less-energy-intensive chemical EOR (cEOR) methods, in which various additives such as polymers,[5,6] surfactants,[7,8] and nanoparticles are used in aqueous solution to alter the oil–water interfacial tension or the wetting characteristics of the rock surface.

Much of the recent research on cEOR has focused on nanofluids, in which surface-interface active nano-sized solid inclusions are used to enhance the effectiveness of oil displacement. There are myriad possible nanofluid formulations using 0D nanoparticles (in which no dimension is greater than 100 nm), 1D nanorods or tubes, and 2D nanosheets with various surface functionalities or charges.[9,10] Silica nanoparticles are among the most popular platforms for formulation of nanofluids because of their commercial availability and ease of surface modification. For example, tuning the surface charge of silica nanoparticles can change a calcite surface from oil-wet to water-wet and accelerate the the dewetting rate of hexane.[11]

Several studies incorporating the use of 2D nanosheets have also been reported. These offer advantages such as improved surface coverage and protocols for modifying each side of the sheet with different chemical functionalities. In one example, Janus graphene oxide (GO)-based nanosheets are functionalized with a polar group on one side and a nonpolar group on the opposite side, such that the sheets aggregate at the oil–water interface and interfacial tension is reduced.[12] Another GO-based nanosheet was demonstrated to alter the wettability of glass and induce a climbing film.[13]

1.3 Focus of This Work

The financial incentive associated with successful EOR operations has provided motivation for a large body of research in this area, including nanofluids. Leveraging this knowledge for decontamination technology development aimed at

addressing capillary features could save time and resources on the development effort. This work specifically examines the effectiveness of two types of nanofluid formulations for decontamination: (1) a reactive sodium-based nanofluid and (2) polyethylene glycol (PEG)–silica-based aqueous nanofluids.

The sodium nanofluid developed at the University of Houston (Houston, TX) is made using a two-step process that involves injection of water followed by addition of a suspension of sodium nanoparticles in silicone oil. Reaction of the sodium nanoparticles occurs at the silicone oil–water interface and is mediated by the immiscibility of the two phases, which controls the rate of reaction, as shown in Figure 2. The reaction produces heat, hydrogen gas, and sodium hydroxide, all of which contribute to oil displacement in EOR. Specifically, heat generation lowers the oil viscosity and the oil–water interfacial tension. Sodium hydroxide can also lower interfacial tension and promote oil emulsification, and the growth of hydrogen bubbles induces a pressure that can push against trapped oil.[14] Experiments on heavy oil sands demonstrated that the sodium nanofluid improved the oil recovery over a control case by approximately a factor of six.[15] For contaminants in capillary features, it was hypothesized that the generation and growth of gas bubbles may provide sufficient pressure to push the contaminant from the capillary.

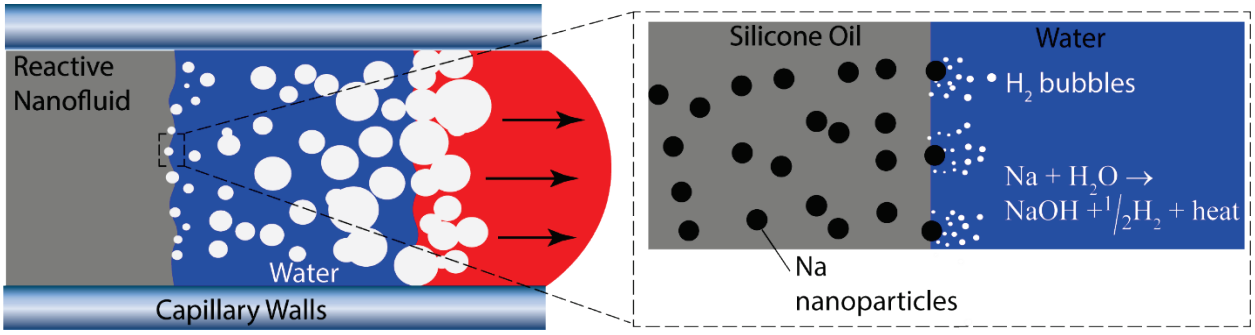

Figure 2. Sodium nanofluid mechanisms of action showing hydrogen gas bubble formation at the silicone oil–water interface due to reaction of the sodium nanoparticles.

Researchers at the Illinois Institute of Technology (Chicago, IL) have published a series of papers spanning over a decade on the development of a nanofluid that promotes dewetting from solid surfaces. The mechanism of action relies on layering of nanoparticles or polymer coils in an aqueous wedge film between the liquid being removed and the solid surface, as shown in Figure 3. This layering increases the structural component of the disjoining pressure[16] in the wedge film and accelerates the dewetting process relative to a pure fluid.[17,18] Key to this mechanism is a sufficiently low water–oil–solid contact angle for wedge film formation and the ability of the particles or polymer coils to form layered structures, which often requires the use of an appropriate surfactant.[19] Zhang et al.[20] clearly laid out additional nanofluid design criteria, namely, that (1) nanoparticles should be small and monodisperse, so that they can form layers inside the wedge film; and (2) the osmotic pressure of the nanofluid should be high, requiring a high concentration of nanoparticles (i.e., >10 vol%). This class of nanofluid has been investigated for cleaning surfaces (i.e., detergency),[21] reducing friction in displacement of a fluid from a capillary,[22] and

recovery of crude oil from sandstone.[20] It is anticipated that, with the appropriate tuning of the nanofluid formulation, the dewetting mechanism would function similarly for CWAs and CWA simulants trapped in capillary features.

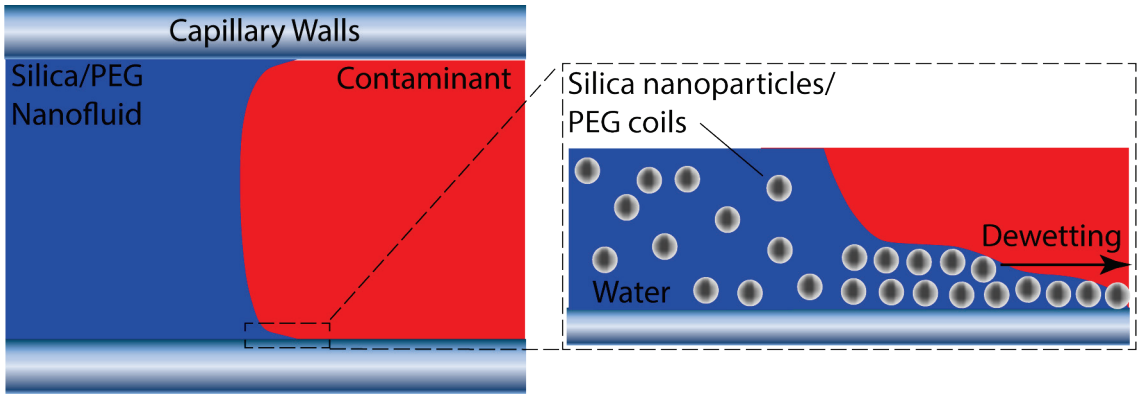

Figure 3. Mechanism of action of nanofluids, based on increasing structural disjoining pressure. Layering of the nanoparticles in the wedge film region occurs as a contaminant dewets from a capillary wall.

2. MATERIALS AND METHODS

2.1 Materials

Of primary interest for this work are the traditional agents sulfur mustard (HD) and *O*-ethyl-*S*-(2-diisopropylaminoethyl) methyl phosphonothiolate (VX). Simulants for these CWAs were also identified to enable visualization experiments outside of engineering controls. Specifically, 1-chlorooctane (product no. 125156; Sigma-Aldrich; St. Louis, MO) and 1,8-dichlorooctane (product no. 361283; Sigma-Aldrich) were identified as simulants for HD, and silicone oil (product no. 378321; Sigma-Aldrich) was selected as a simulant for VX. Table 1 summarizes the CWAs and simulants along with the critical properties surface tension and viscosity. Dyes were used to aid with the visualization of the simulants. Specifically, Fluorosol Red 7348 (Koch Color; Bennett, CO) was used to dye 1-chlorooctane, Fluorosol GR 7200 (Koch Color) was used to dye 1,8-dichlorooctane, and BODIPY 505/515 (Thermo Fisher Scientific; Waltham, MA) was used to dye silicone oil.

Table 1. CWAs and Simulants Used in This Study and Their Relevant Properties

Chemical	Viscosity (cP)	Surface Tension (dyn/cm)	Density (g/cm^3)
HD	~5	~43	1.27
VX	~10	~22	1.01
1-Chlorooctane	1.24	~26	0.875
1,8-Dichlorooctane	~3	36	1.03
Silicone oil	10	~20	~0.90

Sodium nanofluid suspensions (consisting of 10 wt% sodium nanoparticles in silicone oil with viscosity 10 cSt) were supplied by the University of Houston. They were prepared by mechanically mixing sodium with silicone oil. Additional details are provided in prior publications.[13,14] CAUTION: When silicone oil does not sufficiently coat and protect the particles, sodium nanoparticles can react violently with water or humid air to create a potential ignitability hazard.

Aqueous surfactant solutions were prepared above and below the critical micelle concentrations (CMCs) using the anionic surfactant sodium dodecyl sulfate (SDS; product no. 436143; Sigma-Aldrich; CMC of 0.008 M); the cationic surfactant dodecyl trimethylammonium chloride (DTAC; product no. 44242; Sigma-Aldrich; CMC of 0.02 M); and the non-ionic surfactant Tergitol 15-S-9 (product no. 15S9; Sigma-Aldrich; CMC of 39 ppm).

Aqueous PEG solutions with average M_w of 8,000 g/mol (product nos. PHR2894 and 89510; Sigma-Aldrich) were prepared by dissolving in-house deionized (DI) water to make PEG-based nanofluids. Ludox SM colloidal silica (7 nm particle size) in water (product no. 420794; Sigma-Aldrich) was used to make silica-based nanofluids. In some PEG and silica nanofluid formulations, the surfactants identified herein were added at concentrations both below and above the CMC of the respective surfactant.

2.2 Methods

Two capillary geometries were used to assess the performance of the different nanofluids under investigation: a rectangular capillary and a radial capillary. A rectangular capillary with cross-sectional dimensions of 0.05 × 1.0 mm (catalog no. 50-335-61; Electron Microscopy Science; Fisher Scientific) or 0.1 × 2 mm (catalog no. 50-335-63; Electron Microscopy Science) was connected to fluid reservoirs at each end, sealed, and placed on a DVM6 digital microscope stage (Leica Microsystems; Wetzlar, Germany) for observation. Dyed simulant was placed in one reservoir, and the simulant filled the capillary as shown in Figure 4a. The test fluid (e.g., nanofluid) was then deposited in the opposite reservoir, and displacement of the simulant was observed and recorded by the microscope. The radial capillary consisted of two 25 mm diameter glass cover slides (catalog no. 12-545-102P; Fisher Scientific) with their centers offset, which were separated with a 50 μm washer (part no. 98126A161; McMaster-Carr; Atlanta, GA) and bonded with a UV cure glue (Loctite AA 349; Henkel Corporation; Düsseldorf, Germany) as shown in Figure 4b. The radial capillary was placed on the microscope stage for observation. The contaminant (1–5 μL) was deposited at the capillary entrance, and then the test fluid (10–50 μL) was similarly deposited.

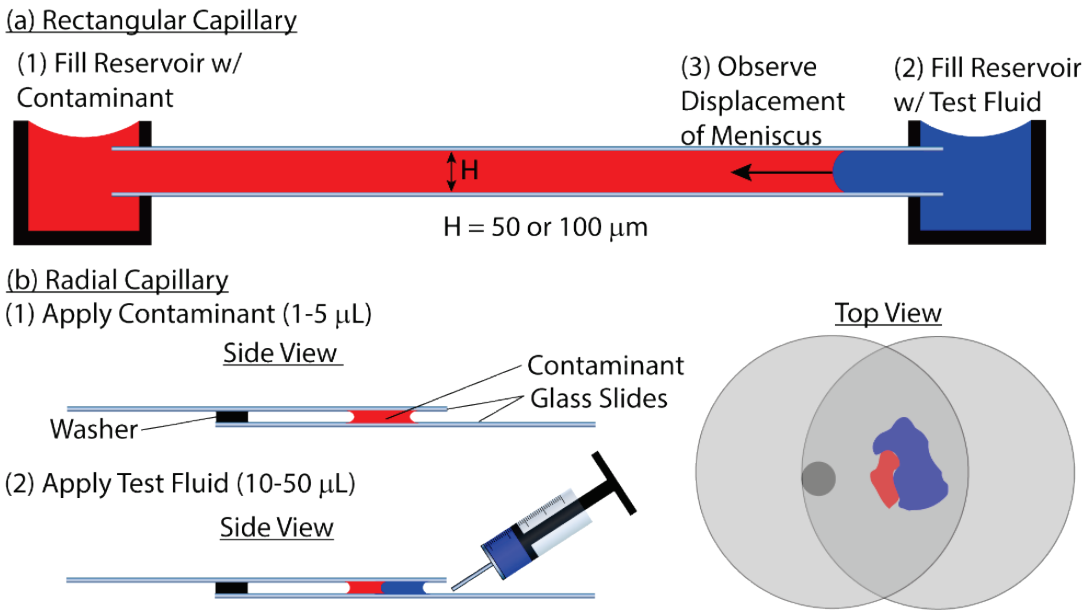

Figure 4. Capillary geometries used in visualization experiments. (a) Rectangular capillary in which one end sits in a reservoir filled with contaminant, and the other end sits in a reservoir filled with test fluid, after the capillary has been filled with contaminant. (b) Radial capillary formed by two circular glass slides and separated by a washer. Contaminant is deposited and then followed by test fluid, to observe displacement.

For CWA experiments, capillaries were constructed from stainless steel washers (both bare and coated with polyurethane-based paint), referred to as shim panels (Figure 5). Additional details on the shim panel methodology are provided in the technical report by Hawbaker et al.[1] In the shim panel configuration, three washers were stacked such that the bottom washer (part no. 90313A105; McMaster-Carr; 0.219 in. i.d.; 1.250 in. o.d.; 0.043–0.057 in. thick) and top washer (part no. 90313A400; McMaster-Carr; 0.203 in. i.d.; 0.750 in. o.d.; 0.033–0.047 in. thick) defined the capillary walls, while the middle shim (part no. 98126A568 ring shim; McMaster-Carr; 0.02 in. thick [20 mil]; 0.25 in. i.d.) defined the capillary spacing. The assembly was compressed by a Phillips flat-head screw (part no. 91099A355; McMaster-Carr; 82 deg countersink; 10-32 thread; 3/8 in. long; undercut) and nut assembly tightened to a torque of 3 in.-lb.

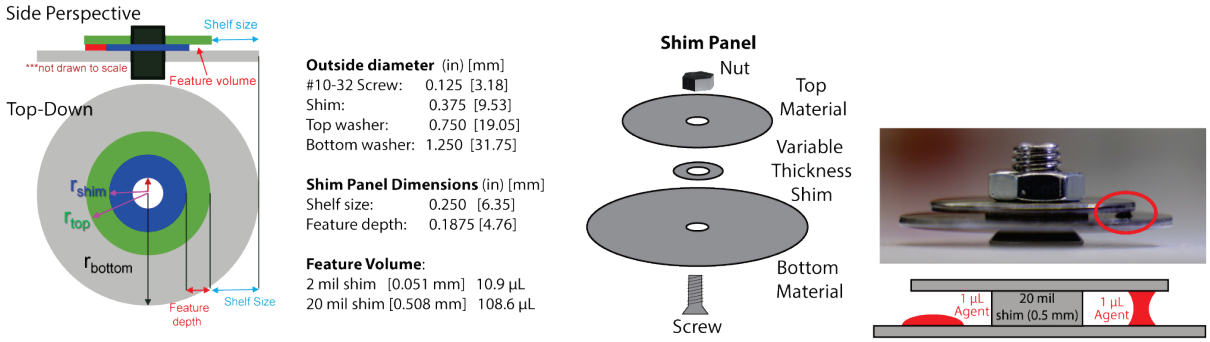

Figure 5. Shim panel shown with dimensions (left) and exploded (middle); and image of contaminated steel panel with 1 µL of liquid contaminant (right). Droplets may or may not bridge the top and bottom materials.

The general procedure for the shim panel is to (1) deposit 1 µL of agent in the capillary; (2) wait 60 min; (3) apply the treatment (e.g., nanofluid); (4) wait 30 min; and (5) rinse three times with 20 µL aliquots of water to remove any accessible agent that was extracted during the treatment process. Both sodium and PEG nanofluids were investigated as treatments. For the sodium nanofluid, 100 µL of water was first deposited and then followed immediately with 50 µL of the nanofluid. For the PEG nanofluid, 50 µL was deposited. Two control cases were also processed: (1) no treatment and (2) no treatment and no rinse. After the contamination and treatment-and-rinse processes, the capillary (shim panel) was immersed in 40 mL of isopropyl alcohol to extract and dissolve any remaining agent trapped within the capillary. Extraction solution samples were diluted, and the analytes were quantified using gas chromatography for HD and liquid chromatography–tandem mass spectrometry for VX. Details on the use of the chromatography platforms are published elsewhere.[23]

3. RESULTS

3.1 Baseline Aqueous Surfactant Solutions

Two concentrations of each aqueous surfactant solution were prepared, one below and one above the corresponding CMC. The contact angle of each surfactant solution (with the glass surfaces of both the rectangular and the radial capillaries) was measured with each simulant. For the rectangular capillary, this involved immersing the end of the capillary in a small droplet of the surfactant solution, wiping excess liquid from the end, and then dipping the same end in a small droplet of the simulant. Figure 6 shows the measured contact angle for each aqueous surfactant solution, including pure water, in a 50 µm rectangular glass capillary with dichlorooctane. Clearly, SDS was the surfactant that most promoted water wetting of the capillary and thus should perform best at displacing contaminant when used in conjunction with a particular nanofluid formulation.

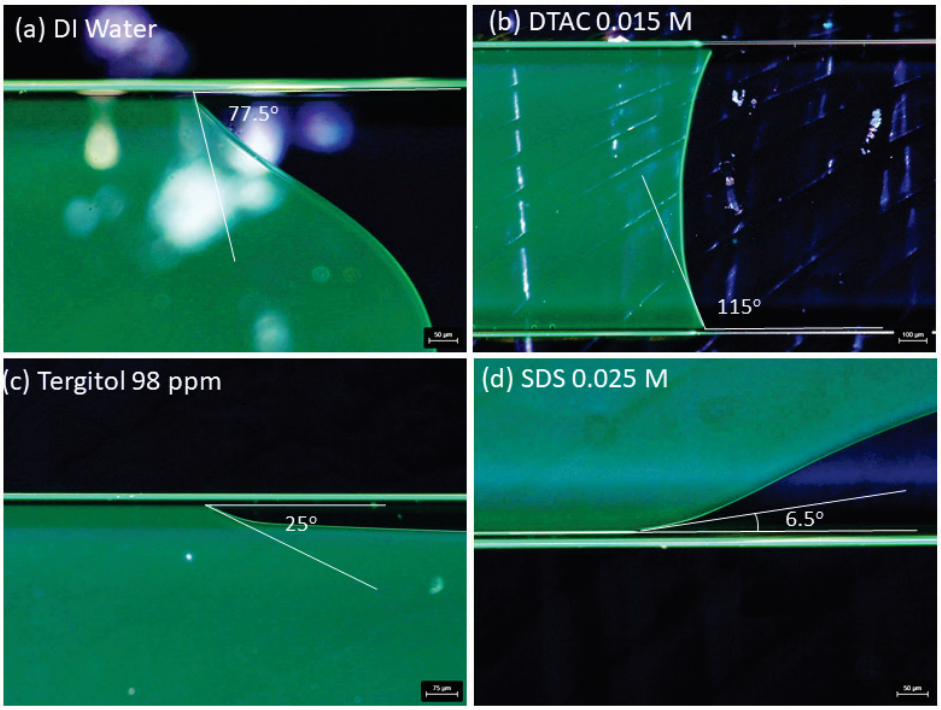

Figure 6. Contact angle of aqueous surfactant solutions in 50 µm rectangular capillary with green-dyed 1,8-dichlorooctane: (a) pure DI water, (b) 0.015 M DTAC, (c) 98 ppm Tergitol, and (d) 0.025 M SDS.

The contact angle was also qualitatively evaluated for each of the aqueous surfactant solutions in contact with the simulants on the glass slide that comprised the radial capillary. This was done by first depositing ~100 µL of the surfactant solution on the glass slide and then depositing 0.5 µL of dyed simulant inside the aqueous surfactant droplet, such that it remained sessile on the glass slide. This is shown in Figure 7 for the simulant 1,8-dichlorooctane, where the droplet diameter was at a minimum within the SDS solution. This indicates that the SDS solution performed best for promoting water wetting on the glass slide, which aligns with the results for the rectangular capillary.

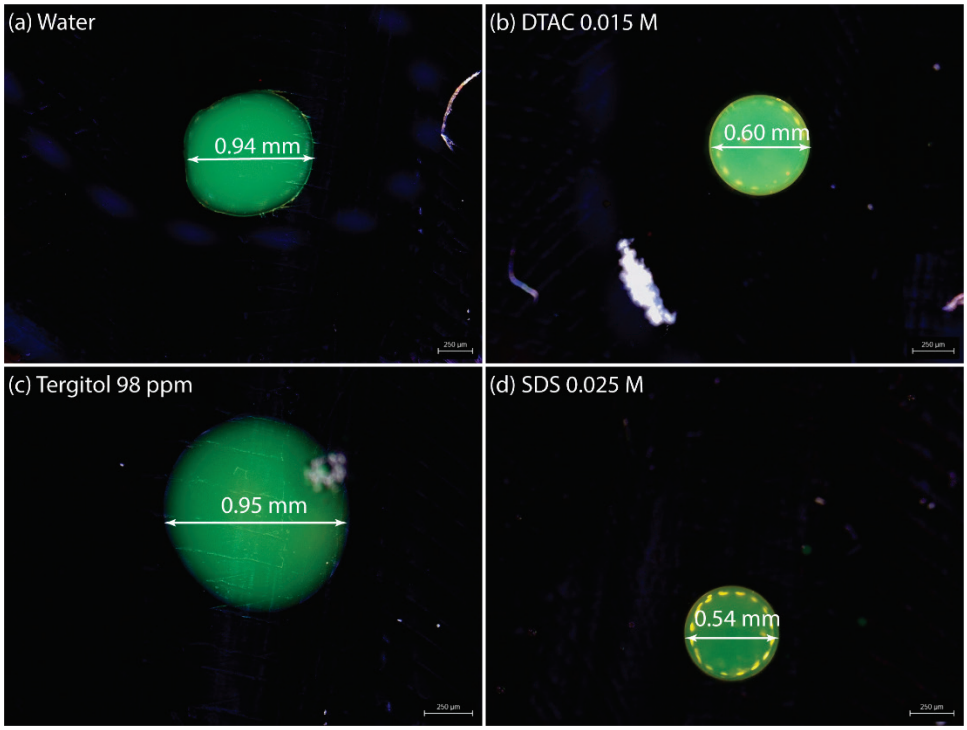

Figure 7. Images of 0.5 µL green-dyed 1,8-dichlorooctane droplets deposited on a glass slide within a 100 µL droplet of (a) pure DI water, (b) 0.015 M DTAC solution, (c) 98 ppm Tergitol solution, and (d) 0.025 M SDS solution.

Each of the aqueous surfactant solutions was used as the test fluid in both the rectangular and radial capillary geometries with each of the simulants. As summarized in Table 2, no displacement was observed for any of the aqueous surfactant solutions with any of the simulants. The simulant did not fill the entire volume of the radial capillary; as a result, some of the aqueous surfactant solution entered the capillary. This resulted in deformation and movement of the liquid simulant within the capillary, but the simulant remained within the capillary.

Table 2. Summary of Visualization Experiments Conducted Using Aqueous Surfactant Controls

Simulants	**Test Fluids**	**Capillaries**	**Results**
1-Chlorooctane 1,8-Dichlorooctane Silicone oil	DI water SDS: 0.008 M, 0.02 M DTAC: 0.02 M, 0.08 M Tergitol: 39 ppm, 98 ppm	Rectangular, 50 µm Radial, 50 µm	No displacement observed for any of the listed combinations

3.2 Sodium Nanofluid

The sodium nanofluid mechanism of action is a two-step process: first an aqueous phase is deposited, then the sodium nanofluid is added to induce reaction of the sodium nanoparticles with water at the silicone oil–water interface. The sodium nanofluid was evaluated using each of the surfactant solutions as the aqueous component in both the rectangular and radial capillaries.

In the rectangular capillary, once the simulant was deposited in one reservoir and the capillary was filled, the aqueous surfactant was deposited in the opposite reservoir. The sodium nanofluid was then deposited on top of the aqueous solution. Displacement was only observed when SDS solutions were used with the nanofluid, as shown in Figure 8a for 1-chlorooctane in a 50 µm rectangular capillary. Gas generation after deposition of the sodium nanofluid is shown on the left side of the image series. Possible mechanisms of action include lowering of interfacial tension and viscosity by heat generation and gas bubble-induced pressure overcoming contact line pinning of the simulant at the entrance to the capillary.

In the radial capillary, the sodium nanofluid effectively displaced the simulant when used in combination with any of the aqueous surfactant solutions, including DI water. Because the entrance to the radial capillary (extending along the perimeter of the top glass slide) was much larger than that of the rectangular capillary, there were multiple pathways for generated gas bubbles to enter and exit the capillary, which provided direct pressure on the trapped simulant. As Figure 8b shows, as time passed, the amount of simulant (green-dyed 1,8-dichlorooctane) in the capillary decreased.

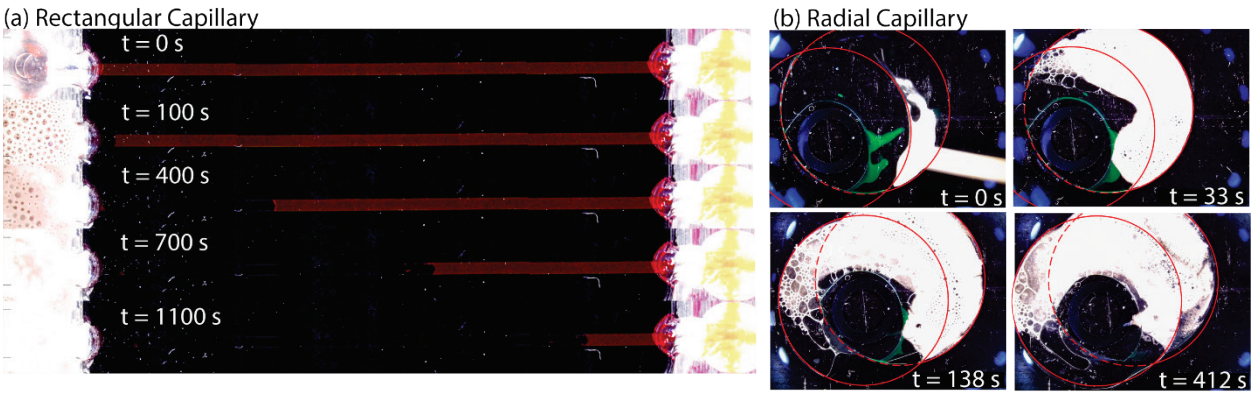

Figure 8. (a) Displacement of red-dyed 1-chlorooctane from 50 µm rectangular capillary using sodium nanofluid with aqueous solution of 0.08 M SDS. At time (t) = 0 s, the SDS solution was in the reservoir (right side of the image), and the sodium nanofluid was deposited over the SDS solution before t = 100 s. (b) Displacement of green-dyed 1,8-dichlorooctane from a 50 µm radial capillary using sodium nanofluid with aqueous solution of 0.08 M SDS. At t = 0, the SDS solution had already been deposited, and it entered the capillary before the sodium nanofluid was deposited. Red lines were added to the images to highlight the periphery of the glass slides forming the radial capillary.

3.3 PEG and Silica Nanofluids

Basic formulation rules for nanofluids operating on the basis of enhanced structural disjoining pressure have been established in a series of papers published by the Illinois Institute of Technology.[20] They specifically found that (1) the water–contaminant–solid contact angle should be as small as possible to promote wedge film formation, (2) nanoparticles should be smaller than 20 nm and monodisperse to effectively layer within the wedge film region, and (3) the osmotic pressure in the nanofluid should be as large as possible. In accordance with point (1), attention was confined to using SDS as a surfactant based on the results described in Section 3.1, which show that SDS produced the smallest contact angle on glass of the surfactants studied here. Dynamic light-scattering experiments performed on dilute aqueous PEG solutions and silica nanoparticle suspensions showed that for the PEG coils, the hydrodynamic diameter (D_h) was ~6 nm, and for the silica nanoparticles, the D_h was ~17 nm. Both exhibited low polydispersity. The volume fraction of the nanofluids (PEG coils or silica nanoparticles) ranged from 0.05 to 0.30, which aligned with studies of similar nanofluids in the literature.[20] Increasing volume fraction further can result in deleterious effects, especially particle–particle interactions and increased viscosity. Table 3 lists the compositions of the PEG and silica nanofluids studied in this work.

Table 3. Aqueous PEG and Silica Nanofluid Compositions

Nanofluid	**Volume Fractions**	**Concentration (mg/mL)**	**Added SDS Surfactant Concentration (M)**
PEG	0.1, 0.2, 0.3	11.8, 23.5, 35.3	0.004, 0.02
Silica	0.05, 0.1, 0.17	110, 220, 374	

Similar behavior was observed for the PEG and silica nanofluids displacing contaminant from a 50 μm rectangular capillary, as shown in Figure 9 for 1,8-dichlorooctane. In both cases, the nanofluid initially dewetted the contaminant on the capillary sides faster than in the middle. This occurred because the cross section of the rectangular capillary is rounded at the sides, which in effect creates a smaller capillary size at the sides and thus a higher capillary pressure driving force for displacement. This effect was not observed in evaluations including the pure SDS solutions, highlighting the efficacy of both the PEG and silica nanofluids for dewetting the contaminant from the capillary walls. However, this efficacy resulted in an undesirable effect: contaminant slugs were pinched off and remained in the rectangular capillary. Note also that the displacement process was slower for the silica nanofluid because of the higher viscosity as compared to that of the PEG nanofluid.

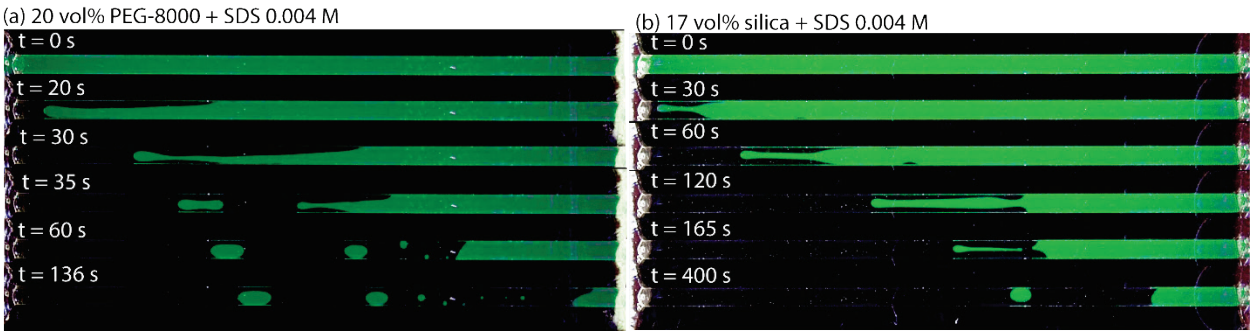

Figure 9. Displacement of green-dyed 1,8-dichlorooctane from 50 µm rectangular capillary using (a) aqueous solution of PEG (20 vol%) and SDS (0.004 M) and (b) aqueous suspension of silica nanoparticles (17 vol%) and SDS (0.004 M).

Figure 10 shows the displacement of 1,8-dichlorooctane from a radial capillary using PEG and silica nanofluids. In both cases, the nanofluid entered the capillary and shifted and distorted the contaminant slug very quickly (<10 s), but it did not exit the capillary. In the case of the PEG nanofluid, some of the contaminant was broken up into small droplets, as shown in the magnified view (Figure 10c).

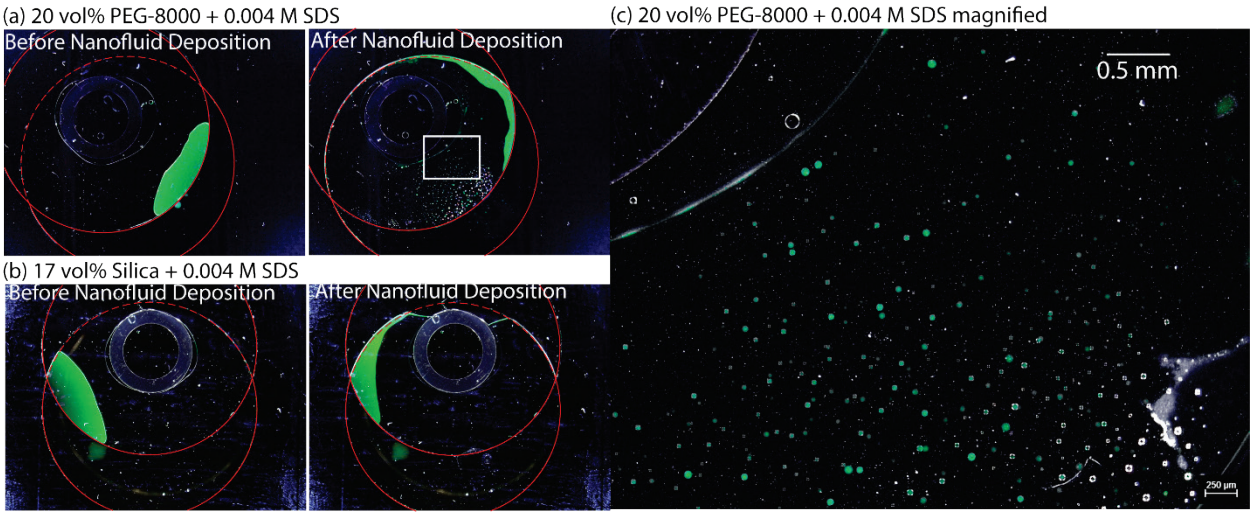

Figure 10. Displacement of green-dyed 1,8-dichlorooctane from 50 µm radial capillary using (a) aqueous solution of PEG (20 vol%) and SDS (0.004 M) and (b) aqueous suspension of silica nanoparticles (17 vol%) and SDS (0.004 M). Red lines were added to the images to highlight the periphery of the glass slides forming the radial capillary. (c) Magnification of area enclosed by white rectangle in (a).

3.4 CWA Testing

The efficacy of the sodium- and PEG-based nanofluids was quantified for removing HD and nerve agent VX from 50 µm shim panels as described in Section 2.2. Figure 11 shows the mass of agent remaining in the capillaries after treatment with the nanofluids in comparison to two control cases, (1) with no treatment and (2) with no treatment and no rinse. The sodium nanofluid effectively removed all HD from bare stainless steel and polyurethane-coated capillaries; however, it demonstrated less efficacy for VX relative to the control cases. The PEG nanofluid was not effective at removing either HD or VX from either type of capillary. These results align with the visual results; namely, that the gas pressure generation of the sodium nanofluid was effective at pushing contaminant from the capillary, and that although the PEG nanofluid was effective at dewetting contaminant from the capillary walls, there was no force causing contaminant removal from the capillary.

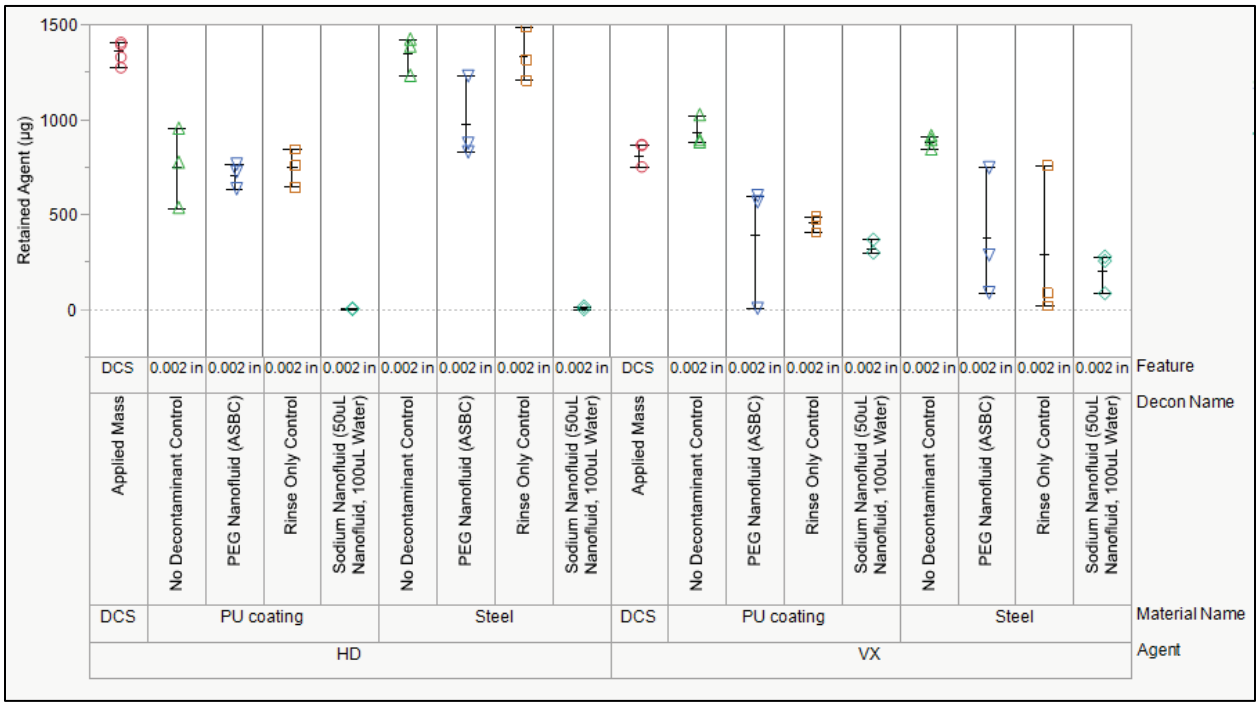

Figure 11. Mass of agent (HD or VX) remaining in 50 µm radial capillary composed of bare or polyurethane (PU)-coated stainless steel. Capillaries were treated with sodium or PEG nanofluid followed by a water rinse to remove any accessible agent that had been displaced. Two control cases were also processed: (1) no treatment was applied, and the water rinse was performed; or (2) no treatment was applied, and no water rinse was performed.

3.5 Silica Nanofluid: Gel Formation and Capillary Extraction

Experiments performed with the silica nanofluids resulted in unexpected behavior that could be useful for extracting contaminant from a capillary. Figure 12 shows the treatment of 1,8-dichlorooctane in a 50 µm radial capillary with a 17 vol% silica nanofluid. The nanofluid filled the remaining volume of the radial capillary, and additional silica nanofluid stayed at the capillary entrance, as denoted by the blue outlined regions in Figure 12. As the water evaporated from the nanofluid, the silica nanoparticles aggregated to form a gel with a pore network morphology dependent on how the nanoparticles packed together, as shown schematically in Figure 13. Because the 1,8-dichlorooctane partially wetted the surface of the silica nanoparticles and the capillary pressure was greater in the pore network than in the radial capillary, the 1,8-dichlorooctane in contact with the silica gel was drawn into the pore network within 20–30 min. This is clearly shown in Figure 12, as the green-dyed area within the radial capillary decreased and the silica gel took on a green hue.

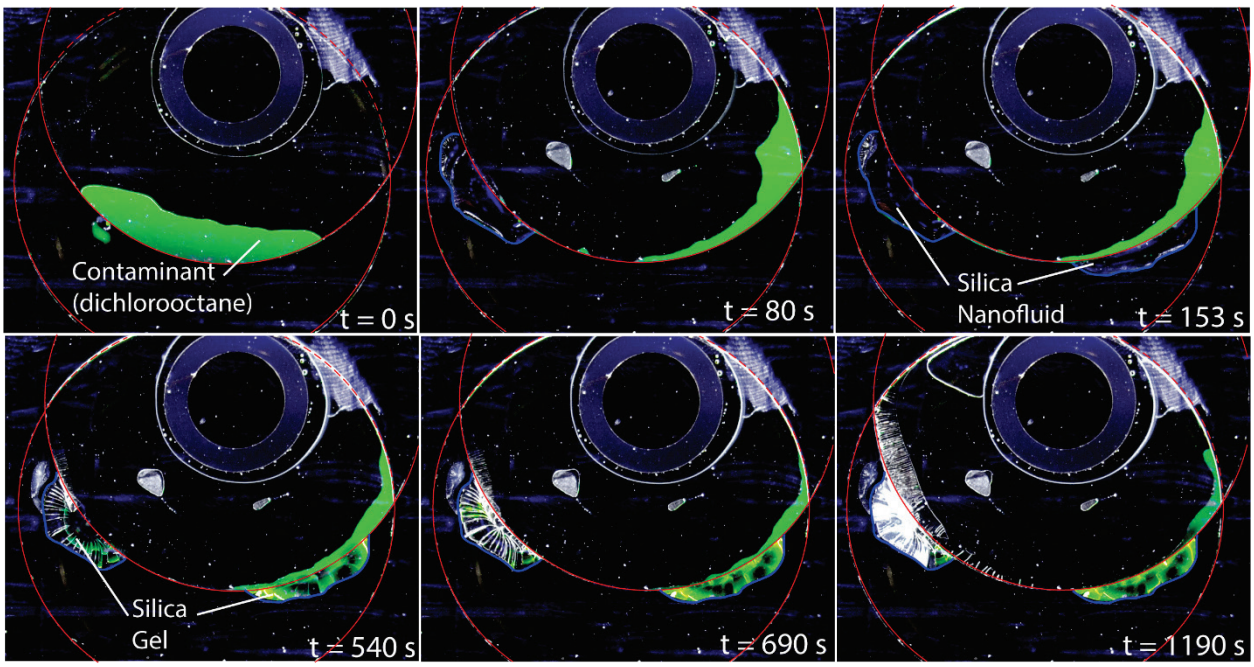

Figure 12. Treatment of green-dyed 1,8-dichlorooctane in a 50 µm radial capillary using 17 vol% silica nanofluid. Image at $t = 0$ s was obtained before deposition of the nanofluid. At $t = 80$ and 153 s, the silica nanofluid had filled the capillary and shifted the 1,8-dichlorooctane. Silica nanofluid outside of the capillary is outlined in blue. From $t = 540$–1190 s, water from the silica nanofluid outside of the capillary evaporated, causing aggregation and gelation of the silica nanoparticles and formation of a pore network. Most of the 1,8-dichlorooctane within the radial capillary was drawn into the silica pore network.

The visualization and CWA results for the PEG and silica nanofluids showed that dewetting and emulsification of the contaminant is not sufficient; there must be a driving force to remove the contaminant from the capillary. The extraction of contaminant into an adjacent pore network driven by a capillary pressure gradient may be a viable passive

mechanism for accomplishing this in practice. Further work is needed to optimize the pore morphology and wetting characteristics as well as the dynamics of the pore formation process. This would involve tuning the size and surface functionalization of the silica nanoparticles in addition to exploring faster gel formation mechanisms, such as altering the pH or ionic strength of the liquid medium.

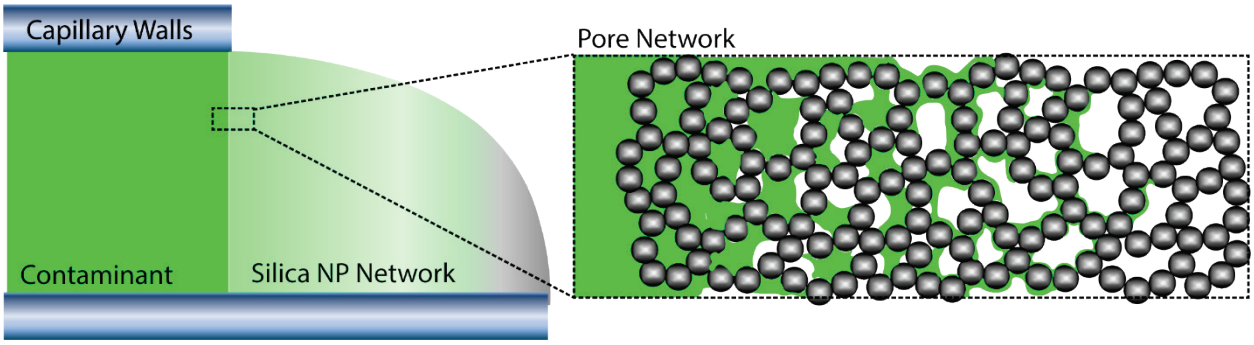

Figure 13. Contaminant extraction from capillary into pore network formed by aggregation of silica nanoparticles (NP).

4. CONCLUSIONS

Two types of nanofluids were investigated for removing contaminants in small capillary features: (1) a reactive sodium nanofluid, and (2) PEG- and silica-based nanofluids that promote dewetting. Visual results showed that the sodium nanofluid effectively pushed contaminant out by formation and expansion of gas bubbles created by reaction with water. However, significant safety concerns exist regarding ignitability of the sodium nanofluid that would prevent its use in the field. Alternative, safer reactive schemes may prove effective but were not investigated here. The PEG and silica nanofluids demonstrated efficacy at dewetting the contaminant from the capillary walls; however, they did not provide a driving force to remove the contaminant in open capillary geometries like the radial capillary studied in this work. Experiments performed with CWAs aligned with the visual results obtained using simulants: the sodium nanofluid was extremely effective at removing HD and somewhat less effective for VX, whereas the PEG nanofluid was ineffective for both agents.

Experiments with the silica nanofluids showed that evaporation of water and the resulting formation of a pore network by gelation of the silica nanoparticles leads to extraction of contaminant from the capillary into the pore network. This passive mechanism relies on a gradient of capillary pressure between the capillary feature and the pore network because of the small pore sizes (capillary pressure is inversely proportional to pore size). Further work is needed to optimize the morphology and wettability of the pore network, in addition to the dynamics of its formation, for its use as an effective decontaminant. Studies should examine the effects of nanoparticle size, concentration, and surface functionalization; the pH and ionic strength of the carrier liquid on the morphology and formation dynamics of the pore network; and the dynamics of imbibition of contaminant into the pore network.

Blank

LITERATURE CITED

1. Hawbaker, N.H.; Mantooth, B.A.; Pearl, T.P. *Effect of Complex Features, Surfaces, and Interfaces on Post-Decontamination Vapor Emission from Contaminated Materials*; DEVCOM CBC-TR-1734; U.S. Army Combat Capabilities Development Command Chemical Biological Center: Aberdeen Proving Ground, MD, 2022; UNCLASSIFIED Report (AD1157423).

2. Druetta, P.; Raffa, P.; Picchioni, F. Chemical Enhanced Oil Recovery and the Role of Chemical Product Design. *Appl. Energy* **2019,** *252*, 43.

3. Mokheimer, E.M.A.; Hamdy, M.; Abubakar, Z.; Shakeel, M.R.; Habib, M.A.; Mahmoud, M. A Comprehensive Review of Thermal Enhanced Oil Recovery: Techniques Evaluation. *J. Energy Resour. Technol.* **2019,** *141* (3) 18.

4. Sheng, J.J. Enhanced Oil Recovery in Shale Reservoirs by Gas Injection. *J. Nat. Gas Sci. Eng.* **2015,** *22*, 252–259.

5. Mahajan, S.; Yadav, H.; Rellegadla, S.; Agrawal, A. Polymers for Enhanced Oil Recovery: Fundamentals and Selection Criteria Revisited. *Appl. Microbiol. Biotechnol.* **2021,** *105*, (21–22), 8073–8090.

6. Gbadamosi, A.; Patil, S.; Kamal, M.S.; Adewunmi, A.A.; Yusuff, A.S.; Agi, A.; Oseh, J. Application of Polymers for Chemical Enhanced Oil Recovery: A Review. *Polymers* **2022,** *14* (7), 39.

7. Massarweh, O.; Abushaikha, A.S. The Use of Surfactants in Enhanced Oil Recovery: A Review of Recent Advances. *Energy Rep.* **2020,** *6*, 3150–3178.

8. Pal, S.; Mushtaq, M.; Banat, F.; Al Sumaiti, A.M. Review of Surfactant-Assisted Chemical Enhanced Oil Recovery for Carbonate Reservoirs: Challenges and Future Perspectives. *Pet. Sci.* **2018,** *15* (1), 77–102.

9. Li, K.W.; Wang, D.; Jiang, S.S. Review on Enhanced Oil Recovery by Nanofluids. *Oil Gas Sci. Technol.* **2018,** *73*, 26.

10. Rezk, M.Y.; Allam, N.K. Impact of Nanotechnology on Enhanced Oil Recovery: A Mini-Review. *Ind. Eng. Chem. Res.* **2019,** *58* (36), 16287–16295.

11. Alzobaidi, S.; Wu, P.K.; Da, C.; Zhang, X.; Hackbarth, J.; Angeles, T.; Rabat-Torki, N.J.; MacAuliffe, S.; Panja, S.; Johnston, K.P. Effect of Surface Chemistry of Silica Nanoparticles on Contact Angle of Oil on Calcite Surfaces in Concentrated Brine with Divalent Ions. *J. Colloid Interface Sci.* **2021,** *581*, 656–668.

12. Zhang, B.; Mohamed, A.I.A.; Goual, L.; Piri, M. Pore-Scale Experimental Investigation of Oil Recovery Enhancement in Oil-Wet Carbonates Using Carbonaceous Nanofluids. *Sci. Rep.* **2020,** *10*, 17539.

13. Luo, D.; Wang, F.; Zhu, J.Y.; Cao, F.; Liu, Y.; Li, X.G.; Willson, R.C.; Yang, Z.Z.; Chu, C.W.; Ren, Z.F. Nanofluid of Graphene-Based Amphiphilic Janus Nanosheets for Tertiary or Enhanced Oil Recovery: High Performance at Low Concentration. *Proc. Natl. Acad. Sci. U.S.A.* **2016,** *113* (28), 7711–7716.

14. Luo, D.; Ren, Z. Synthesis of Sodium Nanoparticles for Promising Extraction of Heavy Oil. *Mater. Today Phys.* **2021,** *16*, 6.

15. Zareei, D.; Luo, D.; Kostrelos, K.; Ren, Z. Sodium Nanofluid for Efficient Oil Recovery in Heavy Oil and Oil Sand Reservoirs. *Soft Sci.* **2021,** *1*, 8.

16. Nikolov, A.; Kondiparty, K.; Wasan, D. Nanoparticle Self-Structuring in a Nanofluid Film Spreading on a Solid Surface. *Langmuir* **2010,** *26* (11), 7665–7670.

17. Kondiparty, K.; Nikolov, A.D.; Wasan, D.; Liu, K.-L. Dynamic Spreading of Nanofluids on Solids. Part I: Experimental. *Langmuir* **2012,** *28* (41), 14618–14623.

18. Liu, K.-L.; Kondiparty, K.; Nikolov, A.D.; Wasan, D. Dynamic Spreading of Nanofluids on Solids Part II: Modeling. *Langmuir* **2012,** *28* (47), 16274–16284.

19. Kondiparty, K.; Nikolov, A.; Wu, S.; Wasan, D. Wetting and Spreading of Nanofluids on Solid Surfaces Driven by the Structural Disjoining Pressure: Statics Analysis and Experiments. *Langmuir* **2011,** *27* (7), 3324–3335.

20. Zhang, H.; Nikolov, A.; Wasan, D. Enhanced Oil Recovery (EOR) Using Nanoparticle Dispersions: Underlying Mechanism and Imbibition Experiments. *Energy Fuels* **2014,** *28* (5), 3002–3009.

21. Wu, S.; Nikolov, A.; Wasan, D. Cleansing Dynamics of Oily Soil Using Nanofluids. *J. Colloid Interface Sci.* **2013,** *396*, 293–306.

22. Wu, P.K.; Nikolov, A.D.; Wasan, D.T. Two-Phase Displacement Dynamics in Capillaries-Nanofluid Reduces the Frictional Coefficient. *J. Colloid Interface Sci.* **2018,** *532*, 153–160.

23. Shue, M.; Lalain, T.; Mantooth, B.; Humphreys, P.; Hall, M.; Smith, P.; Sheahy, M. *Low-Level Analytical Methodology Updates to Support Decontaminant Performance Evaluations*; ECBC-TR-883; U.S. Army Edgewood Chemical Biological Center: Aberdeen Proving Ground, MD, 2011; UNCLASSIFIED Report (ADA546021).

ACRONYMS AND ABBREVIATIONS

cEOR	chemical enhanced oil recovery
CMC	critical micelle concentration
CWA	chemical warfare agent
D_h	hydrodynamic diameter
DI	deionized
DTAC	dodecyl trimethylammonium chloride
EOR	enhanced oil recovery
GO	graphene oxide
HD	sulfur mustard; bis(2-chloroethyl) sulfide
PEG	polyethylene glycol
SDS	sodium dodecyl sulfate
t	time
UV	ultraviolet
VX	*O*-ethyl-*S*-(2-diisopropylaminoethyl) methyl phosphonothiolate

DISTRIBUTION LIST

The following individuals and organizations were provided with one electronic version of this report:

U.S. Army Combat Capabilities Development Command
Chemical Biological Center
(DEVCOM CBC)
FCDD-CBR
ATTN: McDaniel, P.
FCDD-CBR-PD
ATTN: Varady, M.
Mantooth, B.
Morrissey, K.

Defense Threat Reduction Agency
DTRA-RD-IAR
J9-CBS
ATTN: Bass, C.
Higgins, B.

DEVCOM CBC Technical Library
FCDD-CBR-L
ATTN: Foppiano, S.
Stein, J.

Defense Technical Information Center
ATTN: DTIC OA

U.S. ARMY COMBAT CAPABILITIES DEVELOPMENT COMMAND
CHEMICAL BIOLOGICAL CENTER